Oscillations in the NF- B Signaling Pathway

Wang, Yunjiao and Broomhead, David S. and Horton, Caroline A. and Kell, Douglas B. and White, Michael R. H.

2009

MIMS EPrint: **2009.105**

Manchester Institute for Mathematical Sciences
School of Mathematics

The University of Manchester

Reports available from: http://eprints.maths.manchester.ac.uk/
And by contacting: The MIMS Secretary
School of Mathematics
The University of Manchester
Manchester, M13 9PL, UK

ISSN 1749-9097

Oscillations in the NF-κB Signaling Pathway

Yunjiao Wang,University of Manchester,UK
David Broomhead, University of Manchester, UK
Caroline Horton, University of Liverpool,UK
Douglas Kell, University of Manchester, UK
Mike White, University of Liverpool, UK

September 11, 2008

Abstract

NF-κB oscillations were suggested by Hoffmann *et al* from electro-mobility shift assays (EMSA) in population studies of IκB$\alpha^{-/-}$ embryonic fibroblasts and simulated in a computational model. NF-κB oscillations were also observed by Nelson *et al* at the single cell level. The Hoffmann model gave a fairly good prediction of Nelson *et al* oscillatory experimental data using fluorescent proteins. A common comment on the source of oscillations is the existence of negative feedback loops. Just from the point of mathematics, we can set up a simple system containing a negative feedback loop that possesses oscillating behaviour resembling the ones observed in the experiments in the way of Fonslet *et al*. However, in order to understand biological mechanisms, it is necessary to work on models which are detailed enough to relate to biochemical processes and variables measured experimentally even though such models may be very large. In this paper, we are able to analyze the dynamical properties of Hoffmann's computational model (containing 24 variables and 64 parameters), by using a combination of computational and analytical methods, and give an explanation of the source of oscillations. We find that the computational model can be treated as a fast-slow system where the level of total IκB Kinase (IKK) is treated as a slow variable. If the actual variation of IKK is sufficiently slow, then orbits in the true system trace attractors in a family of reduced models. We find that for some range of the level of NF-κB (which is conserved in both the full and reduced models), the reduced system experiences Hopf bifurcations while varying the level of total IKK. The damped oscillations observed in the computational system come from the existence of stable limit cycles and stable spirals in the reduced system family.

1 Introduction

There is an important distinction between the modelling of physical and biological systems which might be characterised in terms of the relevance of Occam's Razor to the modelling process. Consider, for example, the case of circadian clocks [24].

Conceptually, it is easy to construct any one of a number of elegantly simple mathematical models which exhibit autonomous nonlinear oscillations, but in practise, systems biological studies of naturally occurring circadian clocks do not reveal such simplicity. On the contrary, complicated, apparently redundant structure is found, much of which is seemingly irrelevant to the normal working of the organism. There is, as yet, no clear explanation of this phenomenon, although Rand *et al* [24] make an interesting case that such complexity allows for the evolutionary optimisation of multiple objectives.

This phenomenon presents a fundamental—we are tempted to say "philosophical"—difficulty to those who would like to understand the workings of biological systems. The models that arise from experimental studies—which we shall think of as systems of nonlinear, coupled ordinary differential equations—are generally sufficiently complicated that simulation is considered to be the only way understand them. It might reasonably be argued that the result of all the experimental and modelling effort has been to replace one experimental system with another; one in which the role of initial conditions of the system—as well as the uncertainties of a huge number of system parameters—has to be explored and classified.

The intellectual thrust of systems biology is directed towards mathematising biology with the ultimate goal of turning biology into a quantitative science. However, an undervalued virtue of good mathematical modelling is that it provides a rigourous basis for the *qualitative* understanding of systems. In the well-developed quantitative sciences these two views are provided side by side. Generally, good qualitative models are found by wielding Occam's Razor on the fundamental mathematical representation of a system to eliminate small or irrelevant terms and, thereby, produce smaller model systems which capture the essential features of the processes of interest. Mathematicians have engaged in this enterprise by providing precise definitions of qualitative equivalence (see, for example [13]), which allow rigourous conclusions to be drawn as to whether different models exhibit the same qualitative behaviour. These results can often be stated in a way that summarises the behaviour of systems for ranges of initial conditions. Overall, the approach frees the modeller to focus on restricted sets of system parameters at which bifurcations—changes in qualitative behaviour—occur. Moreover, a range of mathematical techniques (for example, Liapunov-Schmidt reduction [11, 12], centre manifold theory [6], a range of singular perturbation techniques [21] as well as various semi-empirical methods which are based on finding nice projections of high-dimensional dynamical systems [2, 9, 14, 4, 5]) have been developed which provide rigourous tools for reducing the complexity of models while still preserving the qualitative behaviour of the original system. From this point of view, simulation need not be the only option when faced with an experimentally-derived model of a biological system. Indeed, qualitative techniques provide synoptic information which compliments and illuminates the results of simulations.

In this paper we will illustrate a way in which these qualitative techniques can be applied to a realistically complicated model system derived from the biology. It will be clear that we are well beyond the regime of back-of-the-envelope calculations here. Applicability of these mathematical techniques requires that they be integrated with computational tools. We have done this at an unsophisticated level, but, nevertheless, we will demonstrate that it is possible to take a reasonably realistic model system

and develop a qualitative understanding of how it functions while retaining contact with the original biologically meaningful representation.

The system we shall study is an oscillatory cell signalling pathway which appears—mathematically at least—to have mechanistic similarities with circadian clocks. This pathway involves nuclear factor (NF)-κB, which comprises of a family of structurally related transcription factors that are involved in regulating numerous genes which play important roles in inter- and intra-cellular signaling, cellular stress response, cell growth, survival and apoptosis.[16]

The rest of the paper is organised as follows. In the next section we describe the background of the NF-κB signalling system and motivate the analysis we use to understand the origins of the observed oscillations. In Section 3, we study a toy model to give a quantitative description of how orbits in a so-called *fast-slow system* trace attractors of the family of systems corresponding to fixed values of the slow variable. In the following sections we consider a model of the NF-kB system based on the work of Hoffmann *et al* [15]. The particular form of this model that we shall use is a reduced version (considering Ihekwaba et al. [18] and assumptions by Nelson et al. [22]). In Section 4, we discuss how the dynamics of this system can be seen as a fast-slow system where the total (complexed and free) level of IκB Kinase (IKK) is treated as a slow variable. In this picture, transient oscillations are understood in terms of a slow tracking through a region of parameter space in which there are Hopf bifurcations. We also develop a simple idea which allows the estimation of the number of observed pulses using information that is naturally obtained from the computational bifurcation calculations. In Section 5, we explore the initial behaviour of the orbits observed in our simulations. This analysis suggests one way in which the phase space of a systems biology model might be structured so as to limit the importance of initial conditions on the ultimate behaviour of the model. We suggest that this is an important issue. The initial state of, for example, a daughter cell after cell division has a random component, it would be surprising if the ultimate fate of the cell were to depend sensitively on this, and yet as we shall show the signal produced by the NF-κB signalling system has a strong dependence on initial condition (see the plots shown in figures 6 and 8 which are for the same model parameter set and differ only in the initial condition used in the integration).

2 The basic ideas about NF-κB signalling

2.1 biological background

In the absence of any stimulus, NF-κB is held within the cytoplasm in an inactive state by association with IκB proteins including IκBα, IκBβ, and IκBε . In response to stimulation, the activated IκB Kinase (IKK) phosphorylates IκB proteins, targeting them for proteolysis through the ubiquitin-proteasome pathway [10]. Phosphorylated IκB proteins are then ubiquitinated and degraded by the proteasome, liberating NF-κB to translocate to the nucleus and regulate target gene transcription. It is of particular interest here that one role of NF-κB is to upregulate the production of IκBα. IκB proteins contain both nuclear localization and export sequences, enabling

its nuclear-cytoplasmic (N-C) shuttling. Newly synthesized free IκB binds to nuclear NF-κB, leading to export of the complex to the cytoplasm [3], becoming a target for the exclusively cytoplasmic IKK [23, 27]. The induction of IκB synthesis by NF-κB, which leads to enhanced export of NF-κB from the nucleus, clearly provides a negative feedback process. More of this will be said below.

Damped oscillations in the temporal response of NF-κB activity (DNA bound nuclear NF-κB) were observed using electromobility shift assay (EMSA) by Hoffmann *et al* who also simulated the behaviour using a mathematical model [15]. Oscillations in NFkB nuclear localisation were also observed by Nelson *et al* [22] at the single cell level using fluorescence microscopy. Numerical integration of the Hoffmann model gave a fairly good prediction of the oscillations observed by Nelson *et al*. However, it would also be satisfying to have a qualitative understanding of how the oscillations arise. For example, is the source of the oscillations associated with under-damped, linear decay to a stable fixed point of the system? Or—since the observed oscillations seem very anharmonic—do we see the effect of a fixed nonlinear transformation of such a decay? Or is it the case that the oscillations are a truly dynamic nonlinear phenomenon? And, if the latter is the case, can we use this knowledge to find a natural way to characterise the observed oscillations?

2.2 modelling philosophy

It is commonly remarked that oscillatory behaviour can be accounted for by the existence of negative feedback loops (under-damped linear decay to a stable fixed point is an elementary example of this—see the illustrative example given in [15]). As a mathematical exercise, it is certainly possible to set up a simple system with a negative—possibly nonlinear—feedback loop which exhibits oscillatory behaviour resembling single cell experimental observations. In a recent paper Fonslet *et al* [8] have done just this. However, different models with different structures can show similar dynamical behaviour. Moreover, our understanding of the mathematics of nonlinear oscillators is such that it is possible for modelling to become a circular exercise, whereby the modeller builds mathematical terms which will give the desired behaviour into the model structure. In such cases it remains a moot point as to whether these terms correspond in any meaningful way to biological mechanisms which are active in the system of interest. We argue that in order to understand a biological mechanism (of NF-κB signalling pathways in this case), it is necessary to work on a model—such as the one considered here—which is based on experimental data. Here we study the dynamical behaviour of the model using a combination of computational and analytical methods. This work will enhance our understanding of the nature of the oscillations manifest by this system. In particular, our approach will provide answers to questions such as those posed at the end of the previous subsection.

2.3 preliminary analysis

From the simulations and experimental results in [15], the system subjected to a continuous stimulus (modelled in the simulation by a slow decay of IKK) exhibits

damped oscillations. A simple explanation of this behaviour would be to suggest that the system has an attracting fixed point when the total concentration of IKK is zero[1]. Let us call this the *quiescent fixed point* for future reference. The damped oscillations would then be understood in terms of the linearisation of the model about the quiescent fixed point. Even though the model has such a fixed point at biologically reasonable values of the system parameters, the derivative (which can be found numerically or by use of computer algebra) of the system of ODEs evaluated at this point is found to have only real eigenvalues in the biologically reasonable parameter range.

Figure 1 summarises the salient features of the eigenvalues of this derivative for the case of the reduced Hoffmann model. We shall return to this figure later, but here we are only interested in the axis total IKK $= 0$ (there are no fixed points of the model when total IKK > 0). It is clear from the figure that the attracting fixed point has only real eigenvalues when total NF-κB < 0.2 (in particular, the eigenvalues are real when total NF-κB $= 0.1$, the value used for the simulations in [15]). This being the case, the evolution of the system to the quiescent fixed point must ultimately be non-oscillatory, and any oscillations that are observed must be intrinsically nonlinear in nature.

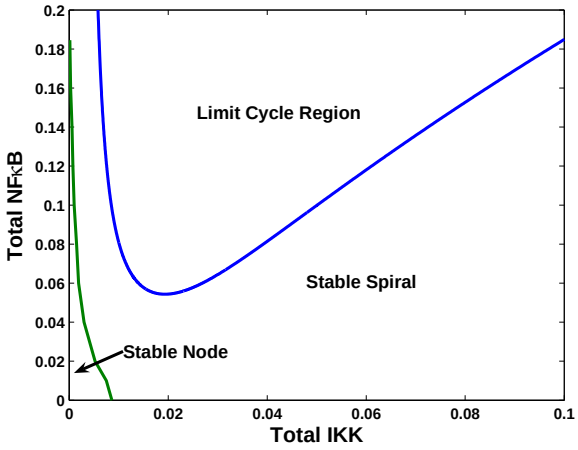

Figure 1: A representation of the important eigenvalues of the derivative of the model evaluated at the quiescent fixed point in the limiting model where total IKK is conserved. Solid green curve: the boundary of region where all eigenvalues are real. Solid blue curve: the Hopf bifurcation line where the real part of the complex eigenvalues change sign.

It appears to be possible that for sufficiently large values of total NF-κB the attracting fixed point can have complex eigenvalues and, therefore, that the signalling system will exhibit damped linear oscillations. However, this is clearly not the case for most of the simulation results reported in the literature.

[1]The modelling will involve only active IKK. In the following 'total IKK' will be used to refer to the overall concentration of active IKK both in its free form and in its complexes. Analogously, we shall refer in this paper to 'total NF-κB' when we wish to account for all the complexed and free NF-κB in the system.

2.4 the fast-slow approach

Horton et al [25] found that in SK-N-AS cells, the temporal response of NF-κB exhibits undamped oscillations when the amount of total IKKremains at some constant level. This suggests that within the state space of the model system, there exists a limit cycle in the subspace corresponding to the fixed level of total IKK. Indeed, since the actual level of IKK is to a degree arbitrary, it suggests that there may be a family of such subspaces, parameterised by a range of values of IKK, in which there exist limit cycles.

Figure 2 shows the result of running a computational bifurcation theory programme on the model of the NF-κB signalling system due to Horton (the corresponding calculation using the Hoffmann model gives closely similar results) taking a limiting form of the model in which total IKK is conserved. What is shown is a

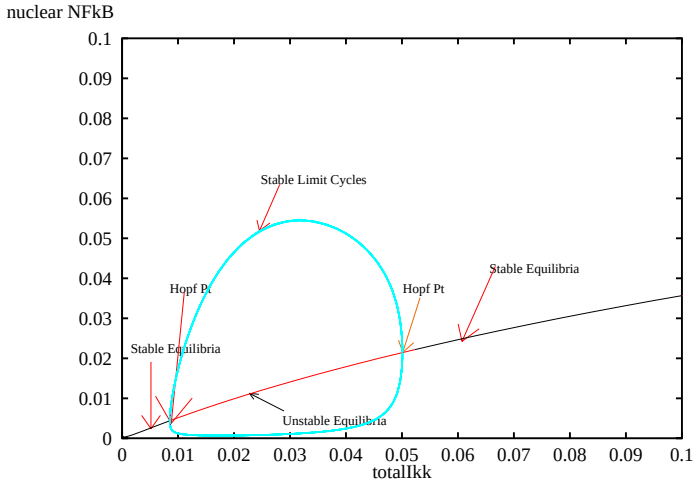

Figure 2: The bifurcation diagram: the solid lines (black lines) represent the branch of stable equilibria, the dashed (red) line represents the branch of unstable equilibria, and the solid curve (green curve) represents the branch of stable limit cycles

projection of a one parameter bifurcation diagram of the system with the level of total IKK as the parameter and with the level of total NF-κB being 0.1[2] The solid lines (black lines) represent the branch of stable equilibria, the dashed (red) line represents the branch of unstable equilibria, and the solid curve (green curve) represents the branch of stable limit cycles (where two points on the same vertical line correspond to the maximum and minimum values of nuclear NF-κB found in one period of the limit cycle). The figure shows that, indeed, if the total IKK is held fixed anywhere in the range ~ 0.01 to ~ 0.05 the system will settle to a stable (undamped) oscillation.

Now let us suppose that the system is initially in the attracting equilibrium state represented by the origin of Figure 2, and assume that an external stimulus is applied to the cell which causes a finite, discontinuous step in the amount of IKK, followed by slow decay. We are interested in the system's response to this input. Following

[2]Neither the Hoffmann nor the Horton models contain a mechanism for the creation or destruction of the NF-κB dimer. Therefore, the total amount of NF-κB (the dimer and its complexes) is conserved in both cases.

the initial discontinuous change in the level of IKK, we expect, intuitively, that if the decay in the amount of IKK is slow compared with the relevant time scales of the rest of the system, the orbits of the true system will trace the limit cycles or fixed points of the one parameter family of systems in which the total IKK is held fixed. A numerical illustration of this in the case of the Horton model with an artificially slow decay rate of IKK is shown in Figure 3 which also shows the original bifurcation diagram (Figure 2) of the system with fixed IKK. In this rather extreme example,

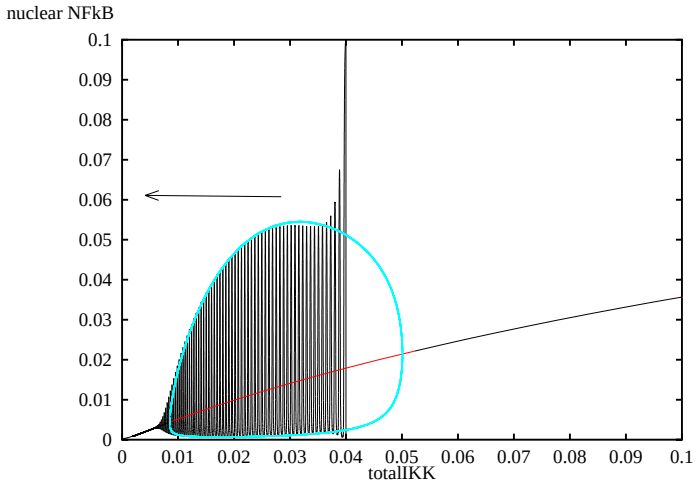

Figure 3: An orbit of the true system with the level of total IKK decaying very slowly is superimposed over the bifurcation diagram.

we can see that orbits of the true system generally trace the attractors of the static system very well.

There are four discernible stages to this behaviour: an initial transient as the system approaches the amplitude predicted by the bifurcation diagram; a period where the oscillation amplitude follows that predicted by the bifurcation diagram; a period of decaying oscillation as the system overshoots the Hopf bifurcation (in this stage, the bifurcation diagram would predict that the system would track the fixed point behaviour); and a period where the system tracks the fixed point and does not oscillate. If we were to plot the time series of, say, the concentration of nuclear NF-κB corresponding to this calculation, the result would be a sequence of (many) pulses whose height generally decays (but not monotonically since having reached the second stage, the amplitude begins to grow in the case shown in Figure 3) until eventually the oscillation disappears to be replaced by a smooth monotone decay to zero.

More realistically, for both Hoffmann's and Horton's models, level of total IKK decreases almost exponentially but not as slowly as was assumed when constructing this illustrative example. For realistic parameter values, therefore, orbits of the true system will not follow the attractors of the reduced system as well in the example. This is illustrated in Figure 4 where we use realistic parameter values. The first peak corresponds to the initial transient, the following three peaks roughly follow the bifurcation diagram, the remaining peak lies in the overshoot region and then the system decays monotonically to the fixed point. Although far from perfect, the agreement is

good enough to provide a reasonable explanation of the oscillating behaviour found in the true system.

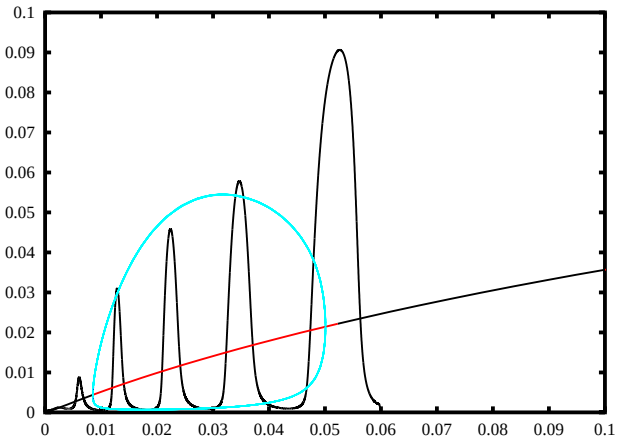

Figure 4: An orbit of the original system is projected to the plane of nuclear NF-κB against total IKK

3 Fast-slow systems

3.1 Hopf bifurcation normal form equations

Before we go on to look in more detail at the NF-κB system, let us pause here to discuss a simple mathematical model which illustrates the properties that we wish to exploit. Consider a system that undergoes a Hopf bifurcation when a parameter, let's say, μ, passes through the fixed value μ_h with nonzero speed. The normal form equations which capture the qualitative behaviour of such a system when $\mu \approx \mu_h$ take the form of a pair of ODEs which can be written in polar coordinates (roughly, think of $r(t)$ as giving the amplitude of an oscillating signal whose phase is $\theta(t)$) as follows:

$$\begin{aligned} \frac{dr}{dt} &= (\mu - \mu_h - r^2)r \\ \frac{d\theta}{dt} &= \omega + \alpha(\mu - \mu_h) + \beta r^2 \end{aligned} \tag{3.1}$$

Here ω is the frequency of small amplitude oscillations of the system at the point of bifurcation. The constant α quantifies the effect on this frequency as μ is varied near the point of bifurcation, and β quantifies the amplitude dependence of the oscillation frequency.

This normal form equation has a skew product structure; we can solve the radial equation separately and then substitute the solution into the angular equation which can then be integrated. The radial equation has two qualitatively distinct types of behaviour depending on the relative magnitudes of μ and μ_h:

A: If $\mu < \mu_h$, then $dr/dt = (\mu - \mu_h - r^2)r < 0$ for all $r > 0$. In this case, therefore, the radial coordinate decreases monotonically in time and in the limit of long times $r(t) \to 0$. Therefore, the origin, $r = 0$, is an attracting fixed point in this case.

B: If $\mu > \mu_h$, there is an attracting radius $r_* = \sqrt{(\mu - \mu_h)}$. If $0 < r < r_*$, then $dr/dt > 0$ and $r(t)$ increases monotonically. Conversely, if $r_* < r$ then $dr/dt < 0$ and $r(t)$ decreases monotonically. In the limit of long times $r(t) \to r_*$, unless initially $r = 0$. The origin is, in this case, an unstable fixed point.

Overall, we see two distinct types of behaviour corresponding to cases **A** and **B**. In case **A**, all solutions of (3.1) with initial conditions $r(0) \neq 0$ are oscillations with amplitude which decays to zero. In case **B**, all solutions are oscillations with amplitudes which evolve towards a stable amplitude, r_*. The resulting stable oscillation has frequency $\omega + (\alpha + \beta)(\mu - \mu_h)$. In both cases there is a fixed point solution $r(t) = 0$. In case **A** this attracts all other solutions, and in case **B** it is repelling.

3.2 a toy fast-slow system

A simple example of a fast-slow system is obtained by augmenting equations (3.1) with a third differential equation which turns the parameter μ into a (slowly varying) dynamical quantity:

$$\frac{dr}{dt} = (\mu - \mu_h - r^2)r \tag{3.2}$$

$$\frac{d\theta}{dt} = \omega + \alpha(\mu - \mu_h) + \beta r^2 \tag{3.3}$$

$$\frac{d\mu}{dt} = -\varepsilon\lambda\mu \tag{3.4}$$

Here ε will be taken to be a small positive number and λ is a decay rate (expressed in units of time^{-1}) which is assumed to have magnitude of order one.

an intuitive picture

Imagine that the original normal form equations evolve on a timescale of seconds. For example, in the regime **B** the rate of contraction, $\lambda_{\mathbf{B}}$, to the stable limit cycle is given by the derivative of the right hand side of the radial equation evaluated at the attracting radius

$$\begin{aligned} \lambda_{\mathbf{B}} &= \frac{d}{dr}(\mu - \mu_h - r^2)r|_{r=r_*} \\ &= -2(\mu - \mu_h) \end{aligned} \tag{3.5}$$

Let us suppose that the time t is expressed in seconds. Then the units of $\lambda_{\mathbf{B}}$ are sec^{-1} and in these units we expect that the magnitude of $\lambda_{\mathbf{B}}$ is number of order one; in other words, the half-life of the decay onto the attracting limit cycle is of the order of one second. A similar argument can be made in case **A** about the decay towards the stable fixed point at the origin. In this case $\lambda_{\mathbf{A}} = -|\mu - \mu_h|$. (Note that in both cases

we have to assume that we are far enough away from the Hopf bifurcation because both $\lambda_{\mathbf{A}}$ and $\lambda_{\mathbf{B}}$ tend to zero as $\mu \to \mu_h$.)

Now we suppose that μ evolves on the timescale of hours (say, $\varepsilon\lambda \sim 3\times10^{-4}$ sec^{-1}). This separation of timescales means that if we compare the half lives of, for example, the convergence to the attracting limit cycle and the decay of μ, that $r(t)$ converges to the limit cycle for many of its half lives but over the same time very little has happened to μ. It is reasonable, therefore, to assume that the radial equation has always converged to the limit cycle at whatever value μ whenever $\lambda_{\mathbf{B}} >> \varepsilon\lambda$. A similar intuitive argument can be made for regime **A** to establish that $r(t)$ converges to the fixed point at the origin whenever $\lambda_{\mathbf{A}} >> \varepsilon\lambda$.

This intuition is often used to justify steady-state approximations when simplifying chemical kinetic systems. Famously, it provides the basis of the derivation of Michaelis-Menten kinetics for enzyme catalysed transformation of a substrate to a product. Perhaps less famously it has a rigourous mathematical basis due to work by A.N. Tikhonov (see the review by Klonowski [20]).

Tikhonov's theorem and a generalisation

Later we shall want to invoke (a generalisation of) Tikhonov's results in the context of the various models of NFκB activity. So here we describe his work in a slightly more formal setting. (The review [20] provides more detail and even more generality than we shall require here.) Consider a system of ordinary differential equations in the following form:

$$\varepsilon\frac{dx}{d\tau} = X(x,y) \tag{3.6}$$

$$\frac{dy}{d\tau} = Y(y,x) \tag{3.7}$$

where ε is a small parameter and the functions $X : \mathbb{R}^n \times \mathbb{R}^m \to \mathbb{R}^n$ and $Y : \mathbb{R}^m \times \mathbb{R}^n \to \mathbb{R}^m$ (where n and m are integers specifying the dimensions of the vectors x and y respectively) are such that the initial value problem consisting of equations (3.6) and (3.7) together with the initial conditions $x(0) = x_0$, $y(0) = y_0$ has a unique solution. Tikhonov studied the relationship between this solution and the solution of the system obtained by setting ε to zero.

Imagine that we find the roots of the equations:

$$X(x,y) = 0 \tag{3.8}$$

and let's say that one of these is $x = f(y)$, that is, $X(f(y),y) = 0$ for all values of y. Then Tikhonov's theorem tells us that when $\varepsilon \to 0$ the solution of equations (3.6) and (3.7) with initial conditions $x(0) = x_0$, $y(0) = y_0$ tends to the solution of the following, so-called *degenerate system*

$$x_* = f(y) \tag{3.9}$$

$$\frac{dy}{d\tau} = Y(y,x_*); \quad y(0) = y_0 \tag{3.10}$$

provided that the following two hypotheses hold:

1. there is a bounded region of $\mathbb{R}^m$ such that for each y in this region, the root $x_* = f(y)$ is an isolated asymptotically stable fixed point of the *adjoined system*

$$\varepsilon \frac{dx}{d\tau} = X(x, y)$$

(here y is treated as a fixed parameter).

2. the initial condition $x(0) = x_0$ lies in the basin of attraction of x_* for all initial values y_0.

In the general setting of the models of NF-κB signalling which we shall consider in this paper the adjoined system will have, rather than a stable fixed point, an attracting limit cycle. In the case of our toy model, the skew product structure of the equations implies that we can still reduce the problem to one of looking for a fixed point. The toy model is valid when we are close to a Hopf bifurcation and therefore we shall use it to illustrate our point. It is possible, however, to generalise Tikhonov's theorem to include the case where the attractor of the adjoined system is more complicated, a limit cycle or even a chaotic attractor, for example. The basic idea of this generalisation is that the dynamics on the attractor of the adjoined system is fast. It is possible, therefore, to average out this rapid variation to give the analogue of the degenerate system which gives the slow dynamics of the system. The paper by Dvořák and Šiška [7] contains a coherent description of this work as well as giving a biologically inspired example.

Tikhonov's theorem applied to the simple model

To apply Tikhonov's theorem to our toy model, we focus on equations (3.2) and (3.4). (The angular equation can be solved separately once we have solved these.) We proceed by rescaling time $\tau = \varepsilon t$ (think of τ being measured in hours and t in seconds). It follows that $d/dt = \varepsilon d/d\tau$, and therefore that we can rewrite equations (3.2) and (3.4) as follows:

$$\varepsilon \frac{dr}{d\tau} = (\mu - \mu_h - r^2)r \tag{3.11}$$

$$\frac{d\mu}{d\tau} = -\lambda\mu \tag{3.12}$$

We are trying to solve these equations—which are in the form of equations (3.6) and (3.7)—given initial conditions $r(0) = r_0$ and $\mu(0) = \mu_0$. A standard result from the theory of ordinary differential equations tells us that there exists a unique solution to this problem[3]. The basic prerequisite for Tikhonov's theorem, therefore, holds.

Now, consider the following system of algebraic and differential equations—the degenerate system—which is obtained formally from equations (3.11) and (3.12) by setting ε to zero:

$$0 = (\mu - \mu_h - r^2)r \tag{3.13}$$

$$\frac{d\mu}{d\tau} = -\lambda\mu; \quad \mu(0) = \mu_0 \tag{3.14}$$

[3]Since the vector valued function $(r, \mu) \mapsto ((\mu - \mu_h - r^2)r, -\lambda\mu)$ is Lipschitz.

In this very simple model the differential equation component (equation (3.14)) of the degenerate system is independent of the algebraic component (given by the roots of equation (3.13)), and can be solved once and for all:

$$\mu(\tau) = \mu_0 e^{-\lambda\tau}$$

The solutions of equation (3.13) are just those given in Section 3.1 where we discussed the Hopf bifurcation. If $\mu < \mu_h$ (case **A**) there is just one relevant root, $r_* = 0$. If $\mu > \mu_h$ (case **B**) there are two relevant roots: $r_* = 0$ and $r_* = \sqrt{(\mu - \mu_h)}$.

In order to apply Tikhonov's theorem we need to check if the two hypotheses given in the previous section hold for these roots. The first hypothesis requires that we can find a bounded interval such that for each μ in the interval the root is an asymptotically attracting fixed point of the adjoined system

$$\varepsilon \frac{dr}{d\tau} = (\mu - \mu_h - r^2)r \tag{3.15}$$

These facts have already been established in Section 3.1 where we discussed the Hopf bifurcation.

In case **A** we can choose any bounded interval which lies within the open interval $\mu < \mu_h$ such that $r_* = 0$ is the attracting fixed point of the adjoined system for any initial condition $r(0) = r_0$. This also establishes the validity of the second hypothesis in this case. Therefore, according to Tikhonov's theorem, if $\varepsilon \to 0$ the solution of equations (3.11) and (3.12) with initial conditions $\mu(0) = \mu_0 < \mu_h$ and $r(0) = r_0$ converges to $(r(\tau), \mu(\tau)) = (0, \mu_0 e^{-\lambda\tau})$.

In case **B** we can choose any bounded interval which lies within the open interval $\mu > \mu_h$ such that $r_* = \sqrt{(\mu - \mu_h)}$ is the attracting fixed point of the adjoined system for any initial condition $r(0) = r_0 > 0$. Again, this also establishes the validity of the second hypothesis and therefore, according to Tikhonov's theorem, if $\varepsilon \to 0$ the solution of equations (3.11) and (3.12) with initial conditions $\mu(0) = \mu_0 > \mu_h$ and $r(0) = r_0 > 0$ converges to $(r(\tau), \mu(\tau)) = (\sqrt{(\mu_0 e^{-\lambda\tau} - \mu_h)}, \mu_0 e^{-\lambda\tau})$ as long as $\mu(\tau) > \mu_h$.

We have established rigourously the result that was argued intuitively in Sections 3.2. The full system (equations (3.2), (3.3) and (3.4)), when $\varepsilon \to 0$, tracks the stable branches of the Hopf bifurcation as long as μ is not too close to μ_h. When $\mu = \mu_h$, Tikhonov's theorem does not hold because the only root of the algebraic part of the degenerate system is $r_* = 0$ and this, although it is a fixed point of the adjoined system, is not asymptotically stable. In practise, when we look at small ε but do not take the limit, there is a region around the Hopf bifurcation point $\mu = \mu_h$ which causes difficulty. We have argued that in this region the timescales of the system are not well separated. In our system if we choose $\mu_0 > \mu_h$ the decay of $\mu(\tau)$ will naturally take the dynamics through this region, therefore we should investigate the behaviour of our toy model to see what we might expect to happen.

the behaviour close to $\mu = \mu_h$

Our toy model is sufficiently simple that we can solve it exactly to establish what happens in the neighbourhood of the bifurcation point $\mu = \mu_h$. Returning to equations

(3.11) and (3.12), if we divide the first equation by the second, we get

$$\frac{dr}{d\mu} = \frac{1}{-\varepsilon\lambda\mu}(\mu - \mu_h - r^2)r. \tag{3.16}$$

We can solve this equation given an initial value of μ, say $\mu_0 > \mu_h$, and a value of

$$r(\mu_0) = r_*(\mu_0) = \sqrt{\mu_0 - \mu_h}$$

which corresponds to the limit cycle tracking behaviour obtained from Tikhonov's theorem. The solution is then a function $r(\mu)$ which gives the extension of the tracking solution into the neighbourhood of $\mu = \mu_h$.

The simplicity of the model resides in the fact that equation (3.16) is a Bernoulli equation. Using the substitution $\tilde{r} = r^{-2}$, the Bernoulli equation can be transformed into a linear, non-autonomous differential equation:

$$\frac{d\tilde{r}}{d\mu} = 2\frac{1}{\varepsilon\mu}[(\mu - \mu_h)\tilde{r} - 1] \tag{3.17}$$

If we choose a sufficiently large value of μ_0—that is, if we start at a point sufficiently far above the bifurcation point—we can write the solution of this transformed equation in terms of the incomplete gamma function $\Gamma(a, x)$ (see Appendix A for the definition of $\Gamma(a, x)$):

$$\tilde{r}_(\mu) = e^{\frac{2\mu}{\varepsilon}}\mu^{-\frac{2\mu_h}{\varepsilon}}(\frac{2}{\varepsilon})^{\frac{2\mu_h}{\varepsilon}-1}\Gamma(\frac{2\mu_h}{\varepsilon}, \frac{2\mu}{\varepsilon}) \tag{3.18}$$

The derivation of this result (given in Appendix A) demonstrates that for sufficiently large μ_0, the value of $r(\mu)$ (or $\tilde{r}(\mu)$) is insensitive to the choice of μ_0. In particular, the value at the Hopf bifurcation point, $\mu = \mu_h$, is independent of the choice of μ_0 and given by

$$r(\mu_h) \approx (\frac{\mu_h\varepsilon}{\pi})^{\frac{1}{4}}. \tag{3.19}$$

if $\mu_h \gg \varepsilon$.

Next we consider how orbits approach the trivial equilibrium after μ passes the Hopf bifurcation point. Since the trivial solution $r = 0$ is attracting, we ignore the higher order term r^2 in the system (3.17). Then we have

$$\frac{d\tilde{r}}{d\mu} = -\frac{1}{\varepsilon\mu}(\mu - \mu_h)\tilde{r} \tag{3.20}$$

Solving this ordinary differential equation we have

$$\tilde{r}(\mu) = e^{-\frac{1}{\varepsilon}(\mu-\mu_0)}(\frac{\mu}{\mu_0})^{\frac{\mu_h}{\varepsilon}}\tilde{r}(\mu_0) \tag{3.21}$$

where $\tilde{r}(\mu_0)$ is a constant of integration.

the overall behaviour

We can now match the two halves of this calculation together—and thereby describe what happens as μ decreases through the region of the Hopf bifurcation—by choosing $\mu_0 = \mu_h$ in (3.21) and using equation (3.19) to set $r(\mu_0) = (\frac{\mu_h \varepsilon}{\pi})^{\frac{1}{4}}$ (that is, $\tilde{r}(\mu_0) = (\frac{\pi}{\mu_h \varepsilon})^{\frac{1}{2}}$) in the above. Then

$$\tilde{r}(\mu) = e^{-\frac{1}{\varepsilon}(\mu - \mu_h)} (\frac{\mu}{\mu_h})^{\frac{\mu_h}{\varepsilon}} (\frac{\pi}{\mu_h \varepsilon})^{\frac{1}{2}} \tag{3.22}$$

We can see from this expression that orbits approach zero as $\mu^{\frac{\mu_h}{\varepsilon}}$ since $e^{-\frac{\mu}{\varepsilon}} \to 1$ as $\mu \to 0$.

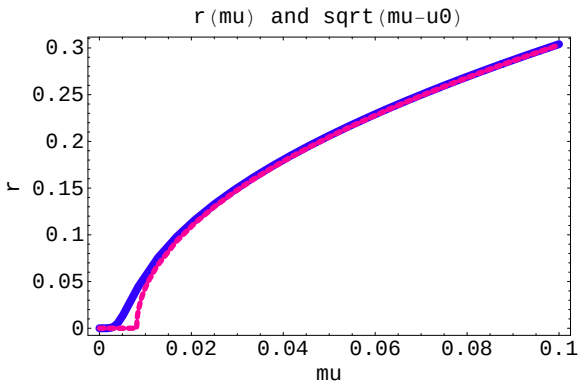

Figure 5: Solid blue curve: plot of $r(\mu)$ found by solving equation (3.16) when $\mu > \mu_h = 0.1$ and when $\mu \leq \mu_h$ and then matching the two solutions using equation (3.19). Dashed pink curve: plot of attracting fixed points of the adjoined system equation (3.15).

Figure 5 summarises these results and provides a comparison with the bifurcation diagram of the adjoined system, equation (3.15). When μ is well away from the Hopf bifurcation value ($\mu_h = 0.1$ in the particular case shown), the trajectories trace the path of the attractors of the system well as is predicted by Tikhonov's Theorem. However, when the parameter is near to the Hopf bifurcation point, the orbit deviates from the path of the attractors and begins to decay towards the origin according to the power law $\mu^{\frac{\mu_h}{\varepsilon}}$. It is clear from the above results that as ε is made smaller the exact solution is approximated increasingly well by the bifurcation curve, nevertheless, for any $\varepsilon > 0$ the power law decay ensures that the full system, equations (3.2), (3.3) and (3.4), continues to oscillate for $\mu < \mu_h$. Our claim is that essentially the same analysis can be used to understand the oscillations in the NF-κB system. From this point of view, this toy model has provided an explicit example of the second and third stages described in the discussion of figures 3 and 4.

4 Dynamical properties of the reduced Hoffmann model

In this section we return to more realistic representations of biological processes and look to see how the abstractions that we have tried to exemplify in the above might be used in practise. We begin by considering the simplification due to Horton [17] of the mathematical model of the NF-κB signalling system proposed by Hoffmann *et al* in [15]. The latter consists of 24 ordinary differential equations and requires the specification of 64 parameters. There are two main points of difference between this and that of Horton. First, the Hoffmann model includes the roles of three IκB proteins: IκBα , IκBβ and IκBε . However, Horton claims that ignoring the effect of IκBβ and IκBε in the model does not destroy the key correspondence of the model output with the experimental data. Therefore, we consider the system (4.1) which is obtained from the Hoffmann's mathematical model with all terms related to IκBβ or IκBε being set to zero. The second difference is that Horton's model replaces the quadratic term in the equation representing IκBα transcription by a linear term. This substitution gives a better prediction of the effect of RelA overexpression. Horton's model is given by the following set of 10 coupled, nonlinear, ordinary differential equations:

$$
\begin{aligned}
y_1' &= k_{d4}\cdot y_3 - k_{a4}\cdot y_2\cdot y_1 - k_{a4}\cdot y_9\cdot y_1 + (k_{r4}+k_{d4})\cdot y_{10} \\
&\quad + k_{deg4}\cdot y_3 - k_1\cdot y_1 + k_{01}\cdot y_4 \\
y_2' &= k_{d1}\cdot y_9 - k_{a1}\cdot y_8\cdot y_2 - k_{a4}\cdot y_2\cdot y_1 + k_{d4}\cdot y_3 \\
&\quad + k_{tr1}\cdot y_7 - k_{deg1}\cdot y_2 - k_{tp1}\cdot y_2 + k_{tp2}\cdot y_5 \\
y_3' &= k_{a4}\cdot y_2\cdot y_1 - k_{d4}y_3 - k_{a7}\cdot y_8 y_3 + k_{d1}\cdot y_{10} + k_2\cdot y_6 - k_{deg4}\cdot y_3 \\
y_4' &= k_1\cdot y_1 - k_{a4}\cdot y_5 y_4 + k_{d4}\cdot y_6 - k_{01}\cdot y_4 \\
y_5' &= k_{tp1}\cdot y_2 - k_{tp2}\cdot y_5 - k_{a4}\cdot y_5\cdot y_4 + k_{d4}\cdot y_6 \\
y_6' &= k_{a4}\cdot y_5\cdot y_4 - k_{d4}\cdot y_6 - k_2\cdot y_6 \\
y_7' &= k_{tr2a} + k_{tr2}\cdot y_4 - k_{tr3}\cdot y_7 \\
y_8' &= (k_{d1}+k_{r1})\cdot y_9 - k_{02}\cdot y_8 - k_{a1}\cdot y_8\cdot y_2 - k_{a7}\cdot y_8 y_3 + (k_{d1}+k_{r4})\cdot y_{10} \\
y_9' &= k_{a1}\cdot y_8\cdot y_2 - (k_{d1}+k_{r1})\cdot y_9 - k_{a4}\cdot y_9\cdot y_1 + k_{d4}\cdot y_{10} \\
y_{10}' &= k_{a7}\cdot y_8\cdot y_3 + k_{a4}\cdot y_9\cdot y_1 - (k_{d1}+k_{d4}+k_{r4})\cdot y_{10}
\end{aligned}
\tag{4.1}
$$

where y_1 = concentration of free cytoplasmic NF-κB ,
y_2 = concentration of free cytoplasmic IκBα ,
y_3 = concentration of cytoplasmic IκBα -NF-κB ,
y_4 = concentration of nuclear NF-κB ,
y_5 = concentration of nuclear IκBα ,
y_6 = concentration of nuclear IκBα -NF-κB ,
y_7 = concentration of IκBα transcript,
y_8 = concentration of free active IKK,
y_9 = concentration of IKK-IκBα ,
y_{10} = concentration of complex IKK-IκBα -NF-κB

and all parameters are determined by measurement or by data fitting [15].

The state space of this model, $\mathcal{S}$, is the closed, positive orthant of $\mathbb{R}^{10}$. That is, at any given time we can specify the state of the system as a 10-dimensional vector whose components—being concentrations—are all greater or equal to zero. If we choose any point in $\mathcal{S}$ as the initial state of the system and solve the system of differential equations subject this initial data, we obtain an orbit in $\mathcal{S}$. This is a curve in $\mathcal{S}$ which depends continuously on the time. Each point in the orbit gives the state of the system at some time following the beginning of the experiment. If, on the other hand, we think of many simultaneous experiments corresponding to a range of initial conditions we can imagine that $\mathcal{S}$ is filled with orbits which because of the uniqueness properties of the differential equations do not intersect one another. As time evolves the states of all the experiments flow as a cloud of points each following its own orbit.

It turns out that there is some hidden simplifications which make the understanding of this system a little easier. In particular, there are *flow invariant subspaces*. These are regions of $\mathcal{S}$ such that if any orbit begins in one of these regions, it must remain in the same region for all time.

4.1 Flow invariant subspaces

The induction of NF-κB activity is not involved in protein synthesis. So if we assume that the volumes of cytoplasm and of nucleus are the same, the concentration of total NF-κB (cytoplasmic and nuclear NF-κB and their complexes) stays constant in the signaling pathway. This conservation law for NF-κB is reflected in the model by the following simple property:

$$\frac{d(\text{total NF-}\kappa\text{B})}{dt} = y_1' + y_3' + y_4' + y_6' + y_{10}' = 0. \tag{4.2}$$

It follows that if we choose a positive real number c, which can be thought of as the total amount of NF-κB (cytoplasmic and nuclear NF-κB and their complexes) found in the system, then the region of $\mathcal{S}$ which intersects the plane $\{y_1+y_3+y_4+y_6+y_{10} = c\}$ is a flow invariant subspace.

Such a flow invariant subspace exists for each choice of c. These are mutually disjoint. Indeed, they are parallel (hyper-)planes, and foliate the whole of $\mathcal{S}$ (rather as we might view a loaf of bread as being made up of its slices). A consequence of this is that for each choice of c we can view the system (4.1) restricted to the corresponding flow invariant subspace as being a different dynamical system. The value of c—the total amount of NF-κB present in the particular system—can be used as a bifurcation parameter of the system.

4.2 The evolution of IKK

The time dependence of total IKK can also be found by adding together the corresponding components of system (4.1)

$$\frac{d(\text{total IKK})}{dt} = y_8' + y_9' + y_{10}' = -k_{02} \cdot y_8 \tag{4.3}$$

This leads to the obvious conclusion that the total IKK is a non-increasing function of time. Indeed, if there is any free IKK present the total amount is decreasing, and the rate of this decay is governed by the constant k_{02}.

In practice, the value used for this constant ($k_{02} \approx 0.007\ \text{min}^{-1}$) will be assumed to be small compared, for example, with the rate of contraction onto the limit cycle solution at some typical fixed value of IKK. In practise, the actual values make this a marginal assumption if are looking for accurate approximations. However, we are interested in finding a qualitative explanation of the observed behaviour. According to this assumption, everything appears to be a response to a slowly decaying input of the IKK stimulus. This suggests that it would be profitable to consider the limiting case where $k_{02} = 0$, where the total IKK is conserved

$$\frac{d(\text{total IKK})}{dt} = 0$$

Now we have the existence of a second family of flow invariant subspaces: $\{y_8 + y_9 + y_{10} = c_1\}$, which is parameterised by a new positive constant c_1, the total IKK. As with the total NF-κB discussed in the previous section, this quantity can be used as a bifurcation parameter of the system when $k_{02} = 0$.

We are now in a position to invoke the fast-slow techniques described in Section 3. Our small parameter—corresponding to ε there—is k_{02}. We shall think of dividing system (4.1) into two parts: equation (4.3); and the remaining part, when we have eliminated one of the variables y_9 and y_{10} in favour of $c_1 = y_8 + y_9 + y_{10}$. In the next section we shall investigate the behaviour of this second part—our adjoined system—when $k_{02} = 0$.

4.3 Bifurcations of the quiescent fixed point

The system given by equations (4.1), when restricted to a particular flow invariant subspace $P_{(c_1,c)} = \{y \in \mathcal{S} : y_1 + y_3 + y_4 + y_6 + y_{10} = c,\ y_8 + y_9 + y_{10} = c_1\}$ is an eight-dimensional system. As such, it is beyond any calculation that could reasonably be carried out by hand. The calculations that we report here were carried out using XPPAUT(X-windows Phase Plane plus Auto) [26] which is a computational tool for solving and analysing systems of differential equations combined with AUTO [1], a package of computational bifurcation and continuation tools.

In the following we shall assume that, initially, the NF-κB and IKK exist only in their uncomplexed forms and, therefore, that c and c_1 are respectively these initial concentrations. Since in the simulations of [15], the initial NF-κB is set to be 0.1, we first consider Horton's reduced system with c being 0.1.

If there is no stimulus, the system stays quiescent. Stimulus in the Hoffmann model was indicated by the activity of IKK. So we begin with finding the equilibrium corresponding to the quiescent state by setting the level of total IKK, c_1, to zero. We then trace the equilibrium while varying the parameter c_1. The bifurcation diagram related to this equilibrium—obtained using XPPAUT—is shown in Figure 2. The equilibrium in the branch remains stable until c_1 is near to 0.01 where it loses its stability and gives way to a stable periodic orbit. The branch of stable periodic orbits exists until c_1 is near to 0.05. For c_1 is greater than 0.05, the branch of

periodic orbits disappears and the branch of equilibria becomes stable again. Figure 2 is the bifurcation diagram projected onto y_4-c_1 plane. Other projections are shown in Appendix B.

4.4 Fast-slow analysis

We have now come full circle, to return to the numerical results shown in Figures 3 and 4. The results of the analysis of the toy model in Section 3 suggest that Tikhonov's Theorem, or its generalisation, can be applied to the Horton model for small values of k_{02}. With this in mind we show a more extensive series of numerical simulations of the Horton model in Figures 6 and 7. These calculations were done to illustrate the effect of changing the initial amount of IKK. (The initial amplitude of IKK would seem to be the simplest possible input to the signalling pathway.) The initial data for these solutions was obtained in the same way as described in the original Hoffmann paper: the initial NF-κB is assumed to be uncomplexed, completely localised within the cytoplasm and set to be 0.1; the system is allowed to converge to an attracting fixed point, and then the value of IKK is reset to a chosen value ($0.02, 0.03, \cdots, 0.1$ respectively).

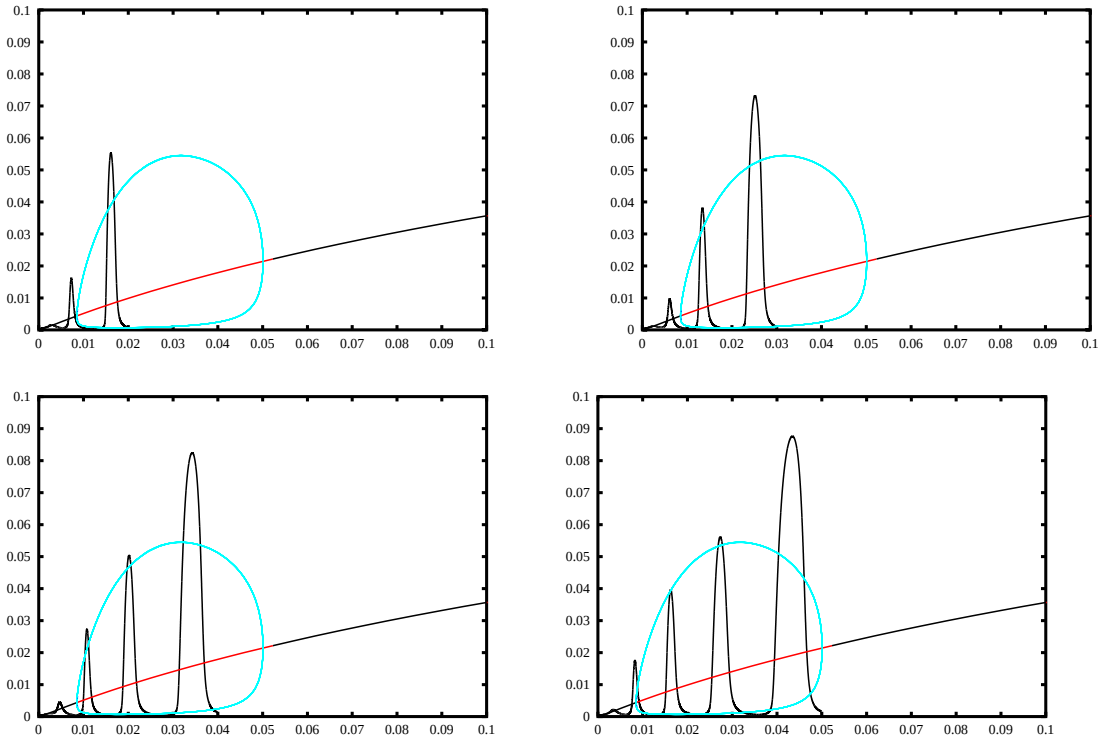

Figure 6: Trajectories with initial total IKK from 0.02 to 0.05, other initial conditions follows Horton's simulation(I)

In figure 6 we see a consistent pattern in which the envelope of limit cycle amplitudes given by the static bifurcation diagram gives a good prediction of the shapes of the pulses obtained by numerical integration of the model. It is worth emphasising

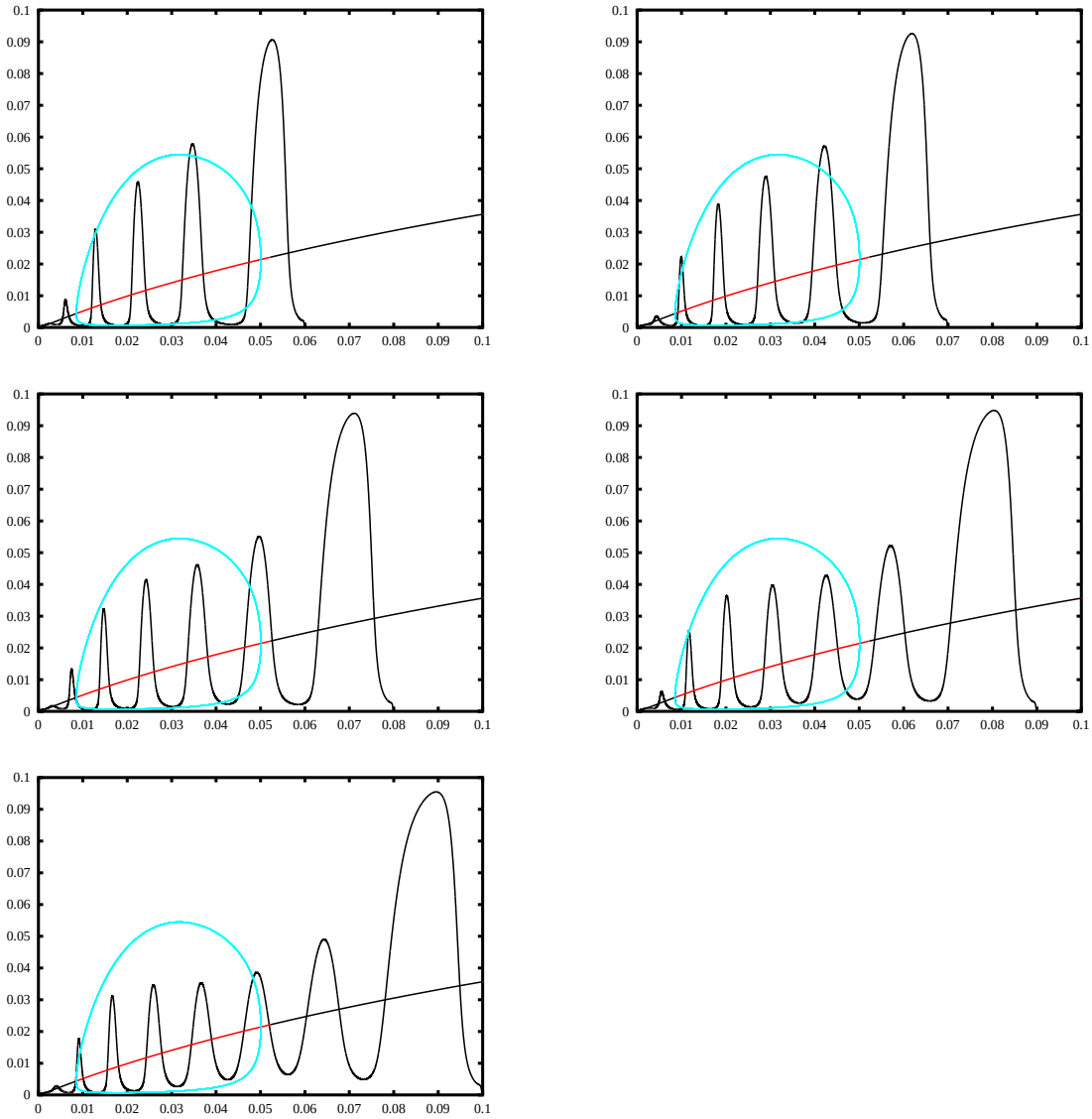

Figure 7: Trajectories with initial total IKK from 0.06 to 0.1, other initial conditions follows Horton's simulation(II)

that this envelope gives both of the obvious characteristics of the pulse shape: the variation in peak height and the level of the flat minimum between the pulses. We have discussed earlier that the first pulse stands out as different, and how we can think of this as being as the major excursion of a transient process as the orbit converges to the form predicted by the fast-slow analysis. Figure 7 shows how this transient can become more significant as the initial value of IKK is increased beyond the second Hopf bifurcation point. All these pulse sequences begin in a region where there is an attracting fixed point in the adjoined system. As the IKK is increased, the effect of this appears to be to hold the orbit away from the bifurcation diagram envelope for longer. In figure 8 we show an extreme example of this behaviour where the initial condition is chosen to be close to the stable fixed point of the adjoined system. Here

the orbit oscillates close to the branch of fixed points. In this case the envelope of the limit cycle amplitudes gives little information about the pulse shapes.

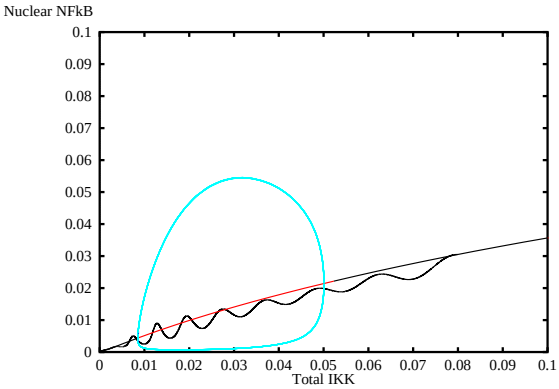

Figure 8: A solution projected to y_4-c_1 plane sticks to the branch of equilibria.

Clearly, this observation suggests that the actual shape, as well as the number of the pulses observed must depend on the initial state of the system[4]. Our results suggest that we can use the fast slow analysis to provide insight into the details of this dependence. The fact that the analysis predicts rapid contraction onto the family of limit cycles of the adjoined system suggests this dependence is more restricted than it might otherwise have been. This would seem to be an important point and we will return to it in the final section.

4.5 estimating the number of pulses

Earlier in this paper, we listed the possible ways that the observed oscillations of the NF-κB system could arise. We have now established that they are intrinsically nonlinear and—although transient—arise through a well-known mechanism which generates autonomous oscillations in nonlinear dynamical systems. Can this insight provide a useful characterisation of the observed oscillations that can be compared with experiments? Of course, we have claimed that to a zeroth order approximation, the shapes of individual pulses are described by the form of the limit cycle of the model at an appropriately fixed value of the total IKK. This could be a useful observation if our purpose is to fit parameters by comparison of experimental and model-derived time series. However, in this section we consider a more basic characterisation: the number of pulses observed.

The calculation we propose is rough-and-ready and should be understood as providing a simple estimate at very little cost. It is based on estimating the total increase in the phase of the limit cycle oscillations as the system slowly tracks through the oscillatory region. Let us call this change $\Delta\theta$. The number of pulses is then obtained from $\Delta\theta/2\pi$ by rounding or truncating to an adjacent integer value.

[4]It is worth remarking that this fact should be born in mind when trying to fit experimental data, since generally there is uncertainty about the initial states represented in the experiment as well as uncertainty in the parameters used to specify the model.

The total change in phase, $\Delta\theta \stackrel{\text{def}}{=} \theta(t_1) - \theta(t_0)$, is the integral of the time derivative of the phase over the time interval, $[t_0, t_1]$, that it takes the system to track through the oscillatory region:

$$\Delta\theta = \int_{t_0}^{t_1} \frac{d\theta}{dt} dt \tag{4.4}$$

(For our purposes we shall interpret the oscillatory region as being the range of total IKK for which there is either a limit cycle solution or—given the observations on overshooting the bifurcation in Section 3— a complex pair of eigenvalues associated with an attracting fixed point of the system.)

Suppose that the adjoined system derived from the Horton model has converged to an attracting limit cycle for some fixed value of c_1. The state of the system on the cycle can be parameterised by the phase angle, $\theta(t)$. The dynamical system restricted to this limit cycle can now be specified by writing $d\theta/dt$ as a function of θ. Although we do not know the explicit form of this function, it may be possible to find a usable approximation because we are only interested in the evolution of θ on the slow time scale associated with the decay of total IKK. The details of $d\theta/dt$ over times less than a single period might, therefore, be considered irrelevant; rather, the average of $d\theta/dt$ over a cycle should suffice.

Let us decompose the derivative, $d\theta/dt$, restricted to the limit cycle, as follows:

$$\frac{d\theta}{dt} = \frac{2\pi}{T(c_1)} + g(\theta) \tag{4.5}$$

where g is a smooth, 2π-periodic function and $T(c_1)$ is the period of the limit cycle at a given value of c_1. We note that if we integrate this expression, assuming a fixed value of c_1, for a whole period then

$$\int_0^{T(c_1)} \frac{d\theta}{dt} dt = \int_0^{T(c_1)} \left[\frac{2\pi}{T(c_1)} + g(\theta) \right] dt \tag{4.6}$$

$$\Rightarrow \theta(T(c_1)) - \theta(0) = 2\pi + \int_0^{T(c_1)} g(\theta) dt \tag{4.7}$$

However, since we have integrated once around the limit cycle, it follows that $\theta(T(c_1)) - \theta(0) = 2\pi$ and, therefore, that the integral of $g(\theta)$ over a whole number of cycles must vanish

$$\int_0^{T(c_1)} g(\theta) dt = 0 \tag{4.8}$$

The $g(\theta)$ component in equation (4.5) is, therefore, a rapidly oscillating term when viewed on the slow time scale on which the total IKK concentration varies. This is a useful result because we can obtain $T(c_1)$ at little cost when using the computational bifurcation package. A plot of $T(c_1)$ versus c_1 is shown in the central portion (between the two Hopf bifurcation points where the slope is discontinous) of figure 9. The two outer portions show the angular frequency associated with the complex eigenvalue of the stable fixed point.

Returning now to equation (4.4), and allowing the slow variation of the total IKK, we have

$$\Delta\theta = \int_{t_0}^{t_1} \frac{2\pi}{T(c_1(t))} dt + \text{oscillatory term} \tag{4.9}$$

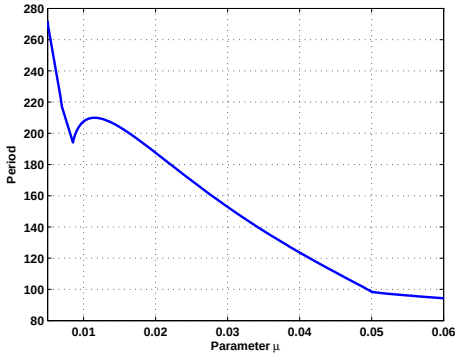

Figure 9: Plot of limit cycle period versus total IKK

We can rearrange this to give an integral with respect to c_1 using the time derivative given in equation (4.3):

$$\Delta\theta = \frac{2\pi}{k_{02}} \int_{c_1(t_1)}^{c_1(t_0)} \frac{dc_1}{T(c_1)y_8} + \text{oscillatory term} \tag{4.10}$$

The rate of decay of the total IKK is governed by y_8, the amount of free IKK.

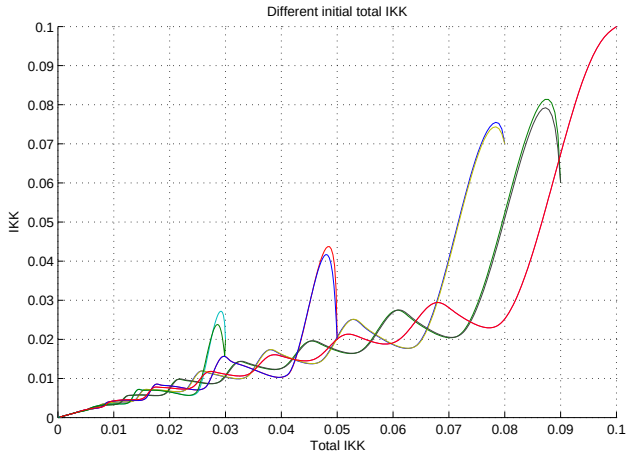

Figure 10: The relationship between total IKK and IKK for different initial conditions but fixed total NFκB

Therefore, we need a relationship between these two quantities. Numerical plots of the y_8 against c_1 obtained by numerical integration of the Horton model are shown in figures 10 and 11. In the first of these, the effect of changing the initial concentration of IKK while keeping all else fixed is demonstrated. We see that to a good approximation:

$$y_8 = \alpha c_1 + \text{oscillatory terms} \tag{4.11}$$

where $\alpha \approx 0.37$, and the linear part of this relationship is independent of the initial concentration of IKK. The main deviation from the linear approximation is the initial transient followed by a damped oscillatory motion which we interpret as being due

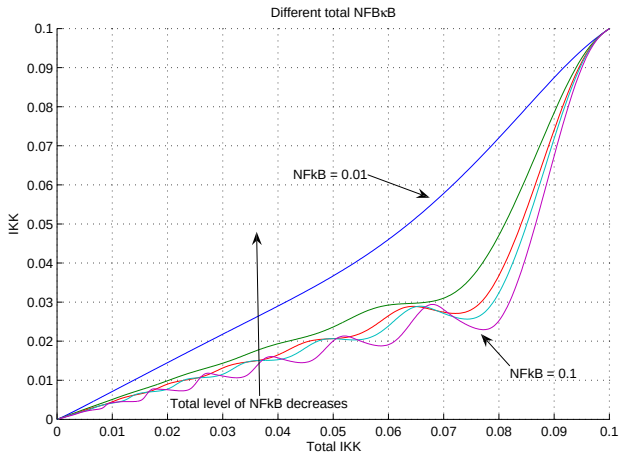

Figure 11: The effect on the relationship between total IKK and IKK for different amounts of total NFκB

motion close to the limit cycle. The second plot shows the effect of changing the total amount of NF-κB while fixing—in particular—the initial value of c_1. Again, we find for each run an approximately linear relationship—modulo the oscillatory component—between c_1 and y_8. In addition, we find that the value of α is a decreasing function of the total amount of NF-κB. Figure 12 shows a number of these runs together with plots of the approximate linear relationship between free IKK and total IKK.

If the oscillatory term is sufficiently small we can rewrite equation (4.10) as follows

$$\Delta\theta = \frac{2\pi}{\alpha k_{02}} \int_{c_1(t_1)}^{c_1(t_0)} \frac{dc_1}{T(c_1)c_1} + \text{oscillatory term} \tag{4.12}$$

We note that in this expression, $c_1(t_0)$ is the initial value of IKK, while $c_1(t_1)$ is the fixed value of the total IKK (given the values of other control parameters such as the total amount of NF-κB) at which the eigenvalue of the stable fixed point below the Hopf bifurcation becomes real. Therefore, by simply varying the $c_1(t_0)$ limit of this integral we are able to estimate the dependence of the number of observed pulses on the initial input of IKK. In figure 13 we show plots of $\Delta\theta/2\pi$ estimated both by using equation (4.10) with numerically obtained values of y_8 and using equation (4.11) with the linear approximation shown in figure 12. In both cases, the actual number of pulses observed in the numerical integration of the full Horton model is plotted for comparison. It is clear from these plots that the effect of using the linear approximation is to smooth out a small modulation of the graph of $\Delta\theta/2\pi$. In either case we have an excellent agreement between the estimate and the actual number of pulses counted from the numerical simulation.

The fact that the agreement seems to be essentially perfect if we use the floor function—the greatest integer less than or equal to $\Delta\theta/2\pi$—requires the injection of some harsh reality. This is an approximation which we expect to work for very small values of k_{02}. In practise, the value of k_{02} used in the simulations is too large to expect dramatic agreement. In addition, we have no good argument for using the

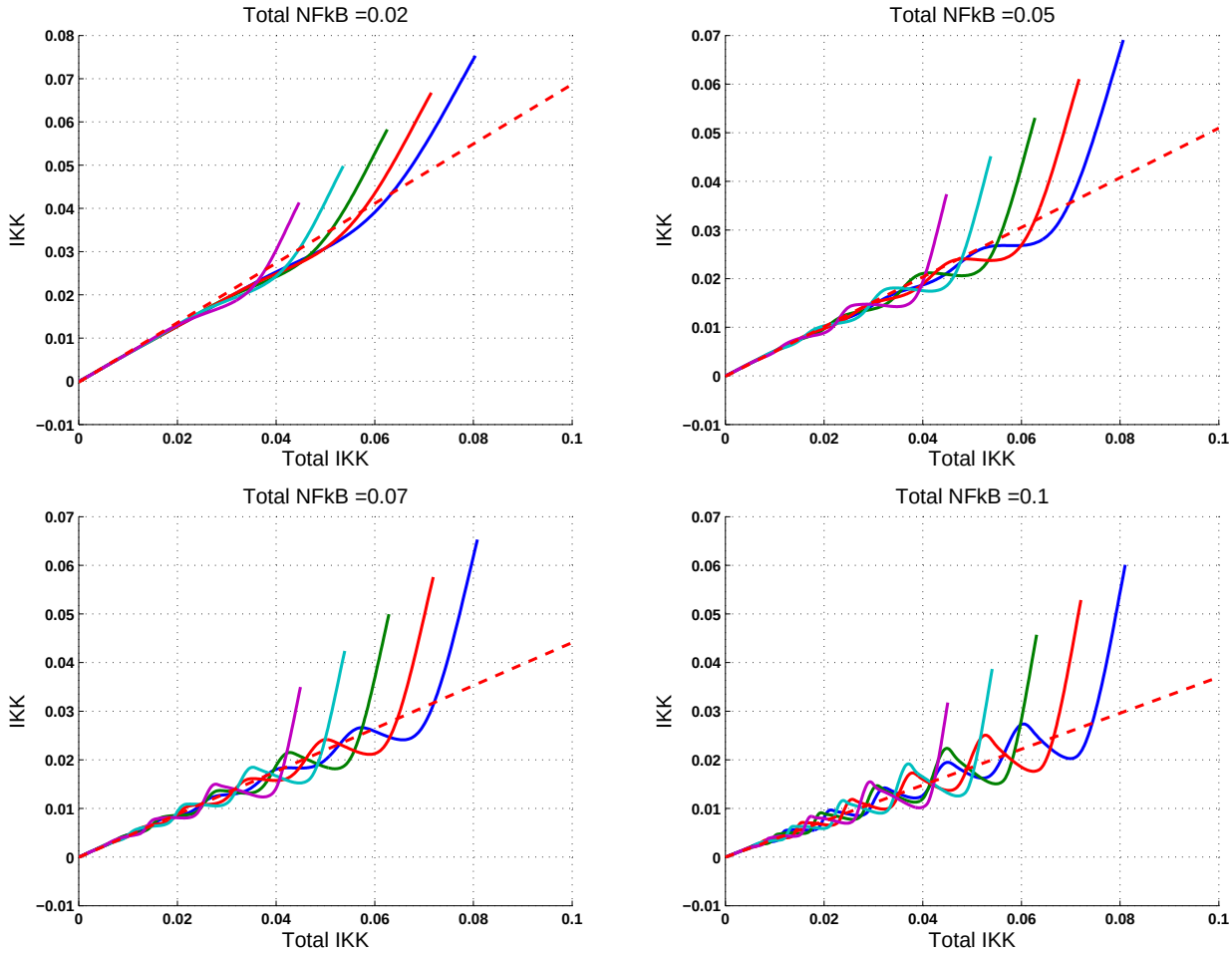

Figure 12: The relationship between total IKK and IKK for different initial conditions, together with the corresponding approximate linear relationship, showing the effect of changing the total amount of NF-κB: Top row left – total NF-κB=0.02; Top row right – total NF-κB=0.05; Bottom row left – total NF-κB=0.07; Bottom row right – total NF-κB=0.1.

floor function to obtain the number of pulses. In fact, we could argue for the ceiling function—the smallest integer greater than or equal to $\Delta\theta/2\pi$—since it is arguable that any cycle begun as the total IKK leaves the oscillatory region will be completed as the system simply decays to the fixed point.

5 Transients and the role of initial conditions

At various places in this paper, we have raised the issue of the role of initial data in determining the behaviour of the model. From the point of view of a mathematician this is such an obvious point that it might seem hardly worth the emphasis, but the initial state of a cell is an extremely difficult idea for the experimentalist. In the first place, it is hard to measure without destroying the cell. Moreover, initial conditions are not tightly controlled as we move from cell to cell, since the detailed profiles of

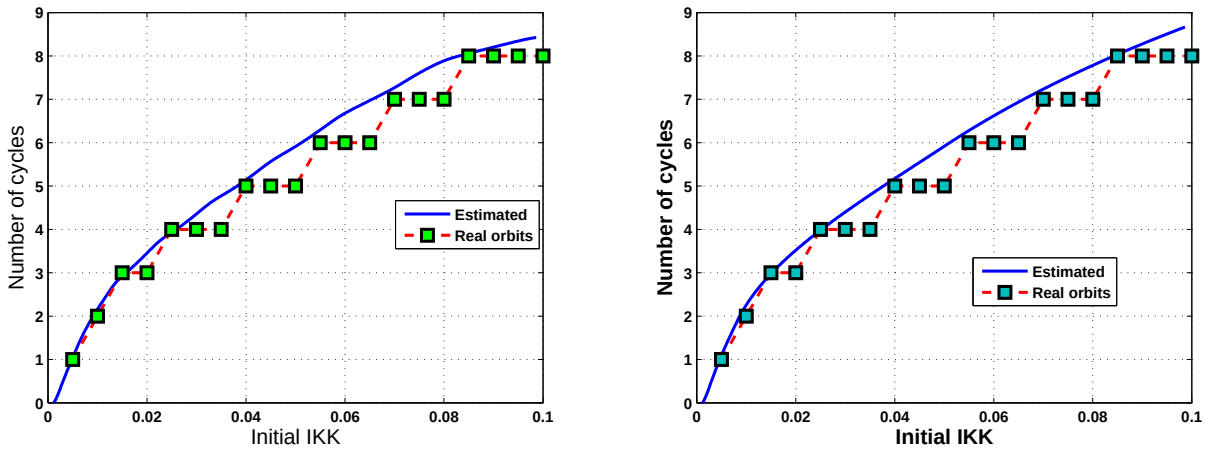

Figure 13: Solid curves: Continuous plots of $\Delta\theta/2\pi$ versus initial value of IKK (Left: estimate using numerical value of total IKK in equation (4.10). Right: estimate using linear approximation for y_8, equation (4.11), in equation (4.10)). Coloured sqares: Actual number of pulses observed in simulation.

concentrations of various chemical species are dependent on the history of the cell; the concentration profile of species present in daughter cells following cell division, for example, appears to be a random sharing of the concentrations present in the parent cell at the mitosis event. *A priori* this means that there will always be an extra layer of uncertainty when trying to compare experimental data with experimentally realistic models. Even with a perfect model—but without knowledge of the initial state—there are likely to be distinct qualitative differences between the behaviour of model and experiment.

The NF-κB signalling system that we have been studying in this paper provides clear examples of this problem. Compare, for example, the responses shown in figure 8 and 7 (middle plot on the left). These represent the response of the system to the same step in the level of IKK, both have the same initial total amount of NF-κB, but have different initial concentrations of the other species. If we suppose that the ultimate fate of the cell depends on the time evolution of the cytoplasm–nuclear shuttling of the NF-κB, this suggests that the fate of the cell might depend on an uncontrolled process associated with the distribution of various species between daughter cells at mitosis. Thus, not only does initial data represent a problem when comparing models with experiments, it also represents a source of variability that—presumably—must at some stage be brought under the control of the cell's systems.

One characteristic of dynamical systems that reduces the dependence on initial conditions is contractivity. Thus, we see in the NF-κB signalling system, the shape and amplitude of pulses shown in figure 6 and the first two figures of 7 are determined by motion close to the envelope of attracting limit cycles of the family of adjoined systems. This is a two-dimensional surface within the corresponding 9-dimensional, flow invariant subspace of $\mathcal{S}$. When near to this surface the only quantities that are of significance are the phase of the oscillation and the current level of the total IKK. Thus, we can argue that the pulses which are well described by motion on this surface

have a shape and frequency which is largely independent of the initial conditions. On the contrary, we have discussed in Section 4, how the first peak of the pulse sequence following the initial stimulus represents a transient response during which the system is far from the envelope of attracting limit cycles of the family of adjoined systems. Thus, we expect that the shape and length of the initial pulse of the sequence is much more dependent on the initial data.

We suggest that there is another way that contractivity can mitigate the effects of variability of initial conditions on such features as the initial pulse of a sequence.

We know that a nonlinear system may have several different equilibria. For Hoffmann's model, we found lots of equilibria by using Mathematica and most of them are far from the region we are interested in. However, a couple of unstable equilibria are near to the reasonable region. So it is possible that the peculiar transient behaviour is caused by the existence of such nearby unstable equilibria. The phase portrait for a two-dimensional nonlinear system in Figure 14 gives an example. In

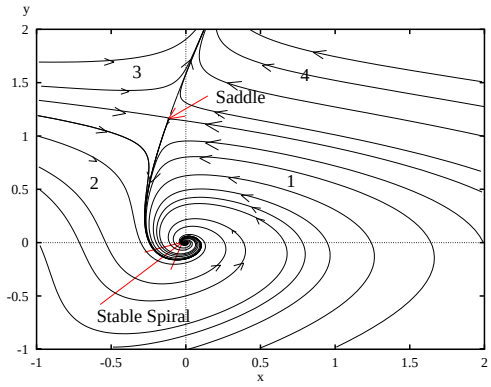

Figure 14: The phase portrait of the system: $x' = -x - 3y - 5xy + 2y^2$; $y' = 3y - y - xy + y^2$

this phase portrait, we can see that the flow of the system is roughly divided by the stable and unstable manifolds of the saddle. Trajectories starting in the same region have the similar dynamical behavior. Trajectories starting in different regions have different behaviour. For orbits starting in the region 1, if the starting point near to the stable manifold of the saddle, the trajectory traces the stable manifold until near to the saddle, then it traces the unstable manifold and then run around the spiral. When the initial point is far from the unstable or stable manifolds, the trajectory is roughly shaped by the stable spiral.

In the NF-κB model, we find those branch of solutions near to the reasonable region are saddle. Orbits starting near to such saddles can run eventually into the reasonable region of the variables. See Figure 15 for an example. Moreover, the Jacobian matrice of the system at the saddles have some very large negative and positive eigenvalues. In the usual simulations, we first let the system converge to a stable state, then set IKK to be some positive value, say 0.1. We argue that the initial condition obtained in this way are near to stable manifold of the nearby saddle. So the dynamical behaviour of the orbit is influenced significantly in the beginning by the saddle.

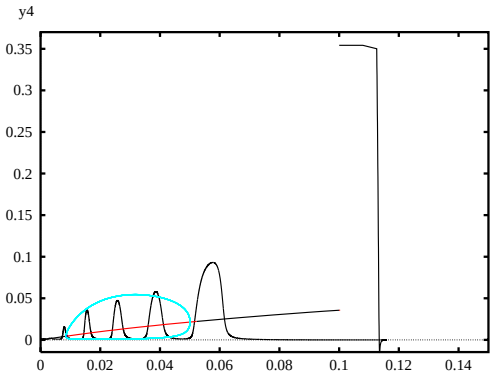

Figure 15: A trajectory (projected to total IKK and nuclear NF-κB plane))runs from an unreasonable region to the reasonable region.

6 Acknowledgement

We thanks the UK BBSRC for financial support.

Appendix A

In Section 3.2 we use the solution of the following Bernoulli equation

$$\frac{dr}{d\mu} = \frac{1}{-\varepsilon\lambda\mu}(\mu - \mu_h - r^2)r. \tag{6.1}$$

given initial data $\mu_h > u_0$ and $r(\mu_h) = \sqrt{\mu_h - u_0}$. In this appendix we show details of the calculation leading to the results quoted in Section 3.2.

There is a well-known way to solve Bernoulli-type equations which employs a simple substitution. Here we write $\tilde{r} = r^{-2}$, to obtain a linear, non-autonomous differential equation:

$$\frac{d\tilde{r}}{d\mu} = 2\frac{1}{\varepsilon\mu}[(\mu - u_0)\tilde{r} - 1] \tag{6.2}$$

Corresponding to this we have a homogeneous equation

$$\frac{d\tilde{r}}{d\mu} = 2\frac{1}{\varepsilon\mu}(\mu - u_0)\tilde{r} \tag{6.3}$$

which can be solved exactly to give:

$$\tilde{r}_h(\mu) = e^{\frac{2}{\varepsilon}(\mu-\mu_h)}(\frac{\mu_h}{\mu})^{\frac{2u_0}{\varepsilon}}\tilde{r}_h(\mu_h) \tag{6.4}$$

where $\tilde{r}_h(\mu_h)$ is a constant of integration.

We can find a particular integral for equation (6.2) as follows

$$\tilde{r}_p(\mu) = -\exp(\int_{\mu_h}^{\mu} 2\frac{\mu - u_0}{\varepsilon\mu}d\mu)\int_{\mu_h}^{\mu}\exp(\int_{\mu_h}^{\mu'} -2\frac{\mu - u_0}{\varepsilon\mu}d\mu)\frac{2}{\varepsilon\mu'}d\mu' \tag{6.5}$$

$$= \frac{2}{\varepsilon}e^{\frac{2}{\varepsilon}(\mu-u_0)}\mu^{-\frac{2u_0}{\varepsilon}}\int_{\mu}^{\mu_h} e^{-\frac{2}{\varepsilon}(\mu'-u_0)}\mu'^{\frac{2u_0}{\varepsilon}-1}d\mu' \tag{6.6}$$

The final integral in this expression is closely related to the incomplete gamma function:

$$\Gamma(a,x) = \int_x^\infty e^{-t}t^{a-1}dt$$

Therefore, we obtain the following explicit formula for the particular integral:

$$\tilde{r}_p(\mu) = e^{\frac{2\mu}{\varepsilon}}\mu^{-\frac{2u_0}{\varepsilon}}(\frac{2}{\varepsilon})^{1-\frac{2u_0}{\varepsilon}}[\Gamma(\frac{2u_0}{\varepsilon},\frac{2\mu}{\varepsilon}) - \Gamma(\frac{2u_0}{\varepsilon},\frac{2\mu_h}{\varepsilon})] \tag{6.7}$$

The general solution to equation (6.2) is obtained by combining the particular integral with the homogeneous solution

$$\tilde{r}(\mu) = \tilde{r}_h(\mu) + \tilde{r}_p(\mu) \tag{6.8}$$

Now, we would like to impose the initial data corresponding to the Tikhonov result. Since it is apparent that $\tilde{r}(\mu_h) = \tilde{r}_h(\mu_h)$, we write $\tilde{r}_h(\mu_h) = 1/(\mu_h - u_0)$. It then follows that

$$\tilde{r}_h(\mu) = \frac{e^{\frac{2}{\varepsilon}(\mu-\mu_h)}}{(\mu_h - u_0)}(\frac{\mu_h}{\mu})^{\frac{2u_0}{\varepsilon}} \tag{6.9}$$

We take μ_h to be large and then consider the form of $\tilde{r}(\mu)$ (and hence $r(\mu)$) as μ approaches the bifurcation point, u_0. In fact, choosing a large value for μ_h, enables us to make equation (6.8) take a simple form. First we note that $\tilde{r}_h(\mu) \sim e^{\frac{2}{\varepsilon}\mu}\mu^{-\frac{2u_0}{\varepsilon}}e^{-\frac{2}{\varepsilon}\mu_h}\mu_h^{\frac{2u_0}{\varepsilon}-1}$ and, therefore, that for any finite value of μ we can choose μ_h which is large enough to make $\tilde{r}_h(\mu)$ as small as we wish. In the same spirit, as $x \to \infty$, the incomplete gamma function has the following asymptotic form:

$$\Gamma(a,x) = x^{a-1}e^{-x}(1 + O(x^{-1}))$$

and, therefore, we can choose μ_h to be sufficiently large to make the term $\Gamma(\frac{2u_0}{\varepsilon},\frac{2\mu_h}{\varepsilon})$ appearing in equation (6.7), the expression for the particular integral, as small as we like:

$$\Gamma(\frac{2u_0}{\varepsilon},\frac{2\mu_h}{\varepsilon}) \sim (\frac{2\mu_h}{\varepsilon})^{\frac{2u_0}{\varepsilon}-1}e^{-\frac{2\mu_h}{\varepsilon}} \tag{6.10}$$

In conclusion, for large enough μ_h, we can write

$$\tilde{r}(\mu) = e^{\frac{2\mu}{\varepsilon}}\mu^{-\frac{2u_0}{\varepsilon}}(\frac{2}{\varepsilon})^{1-\frac{2u_0}{\varepsilon}}\Gamma(\frac{2u_0}{\varepsilon},\frac{2\mu}{\varepsilon}) \tag{6.11}$$

which is the first result used in Section 3.2.

Later in 3.2 we use this form of $\tilde{r}(\mu)$ (or, equivalently, $r(\mu)$) at $\mu = u_0$. The derivation of this result follows from the asymptotic form of $\Gamma(x,x)$ as $x \to \infty$

$$\Gamma(x,x) = \frac{1}{x}e^{-x}x^x(\sqrt{\frac{\pi}{2}}x^{\frac{1}{2}} - \frac{1}{3} + \frac{\sqrt{2\pi}}{24}\frac{1}{x^{\frac{1}{2}}} + \cdots) \tag{6.12}$$

Hence, as long as $u_0 \gg \varepsilon$

$$\begin{aligned}
\tilde{r}(u_0) &\approx e^{\frac{2u_0}{\varepsilon}}u_0^{-\frac{2u_0}{\varepsilon}}(\frac{2}{\varepsilon})^{-\frac{2u_0}{\varepsilon}+1}\Gamma(\frac{2u_0}{\varepsilon},\frac{2u_0}{\varepsilon}) \\
&= e^{\frac{2u_0}{\varepsilon}}u_0^{-\frac{2u_0}{\varepsilon}}(\frac{2}{\varepsilon})^{-\frac{2u_0}{\varepsilon}+1}\frac{\varepsilon}{2u_0}e^{-\frac{2u_0}{\varepsilon}}(\frac{2u_0}{\varepsilon})^{\frac{2u_0}{\varepsilon}}(\sqrt{\frac{\pi}{2}}(\frac{2u_0}{\varepsilon})^{\frac{1}{2}} - \frac{1}{3} + \frac{\sqrt{2\pi}}{24}\frac{1}{(\frac{2u_0}{\varepsilon})^{\frac{1}{2}}} + \cdots) \\
&= \sqrt{\frac{\pi}{u_0\varepsilon}} + o((\frac{2u_0}{\varepsilon})^{\frac{1}{2}})
\end{aligned}$$

and, therefore,

$$r(u_0) \approx (\frac{u_0 \varepsilon}{\pi})^{\frac{1}{4}} \tag{6.13}$$

Appendix B

The projections of a solution and the bifurcation diagram to c_1-y_i ($i \in \{2, 3, 4, 5, 6, 7, 9, 10\}$) plane are in Figure 16, Figure 17 and Figure 18.

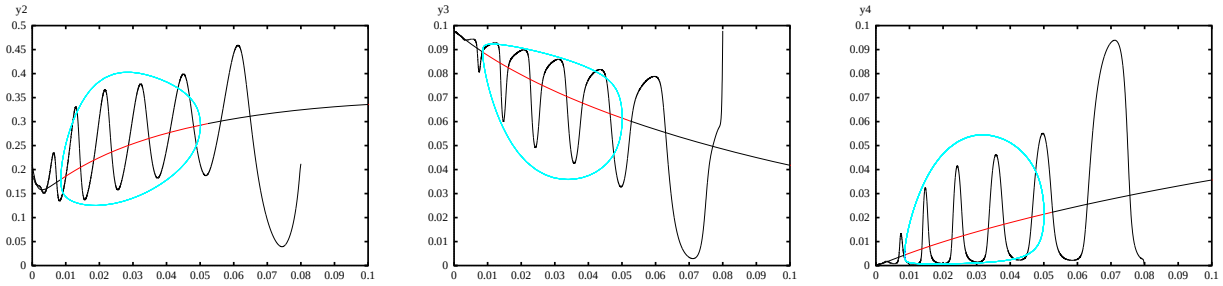

Figure 16: The bifurcation diagram and the solution (I)

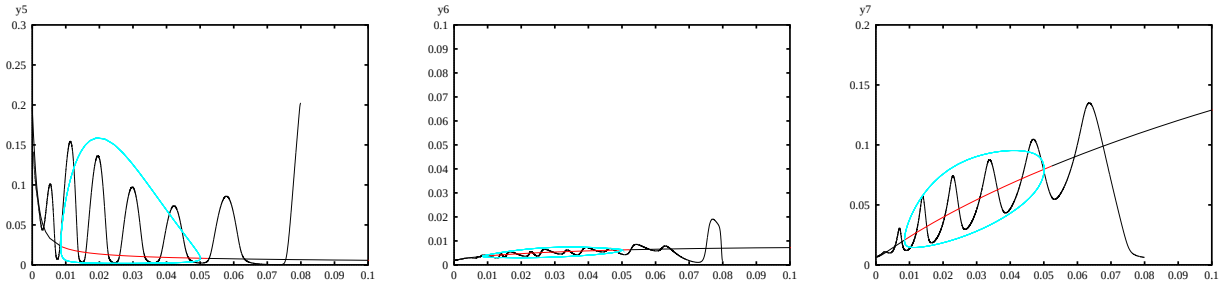

Figure 17: The bifurcation diagram and the solution (II)

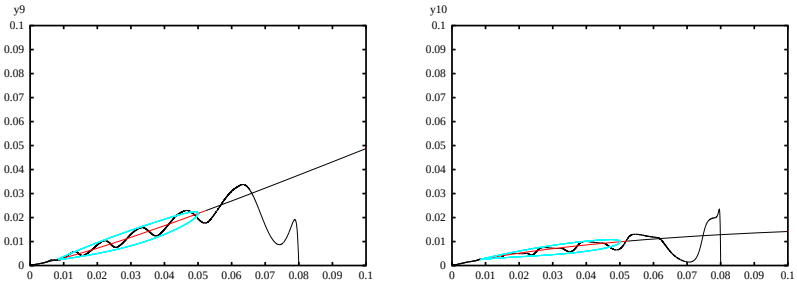

Figure 18: The bifurcation diagram and the solution (III)

References

[1] `http://indy.cs.concordia.ca/auto/`

[2] A.C. Antoulas, *Approximation of Large-Scale Dynamical Systems*, SIAM Philadelphia, PA, USA, (2005)

[3] F. Arenzana-Seisdedos et al., *Mol. Cell. Biol.* **15**, 2689 (1995)

[4] D.S. Broomhead, M. Kirby, *A new approach to dimensionality reduction*, SIAM J. Appl. Math., **60** (2000), 21142142.

[5] D.S. Broomhead, M. Kirby, *Dimensionality reduction using secant-based projection methods*, Nonlinear Dynamics, **41** (2005), 4767.

[6] J. Carr, *Applications of Center Manifold Theory* Springer-Verlag: NewYork, Heidelberg, Berlin, (1981)

[7] I. Dvořák, J. Šiška, *Analysis of Metabolic Systems with Complex Slow and Fast Dynamics*, Bull. Math. Biology, **51**, 255–274, (1989)

[8] J. Fonslet, K. Rud-petersen, S. Krishna, and M. H. Jensen, Pulses and Choas: Dynamical Response in a simple genetic oscillator. *International Journal of Modern Physics B* Vol **21**, Nos 23 & 24, 4083 - 4094 (2007)

[9] K. Gallivan, A. Vandendorpe, AND P. V. Dooren, *Model reduction via truncation: an interpolation point of view*, Linear Alg. Appl., **375** (2003), 115134.

[10] Ghosh, S., May, M.J., and Kopp, E.B.: 'NF-kappa B and Rel protein: evolutionarily conserved mediators of immune responses', *Annu. Rev. Immunol.,* **16**, 225-260 (1998)

[11] Martin Golubitsky, David G. Schaeffer, *Singularities and Groups in Bifurcation Theory I*, Applied Mathematical Sciences **51**, Springer-Verlag: NewYork, Heidelberg, Berlin, (1985)

[12] Martin Golubitsky, Ian Stewart, David G. Schaeffer, *Singularities and Groups in Bifurcation Theory II*, Applied Mathematical Sciences **69**, Springer-Verlag: NewYork, Heidelberg, Berlin, (1988)

[13] John Guckenheimer, Philip Holmes, *Nonlinear Oscillations, Dynamical Systems and Bifurcations of Vector Fields*, Applied Mathematical Sciences **42**, Springer-Verlag: NewYork, Heidelberg, Berlin, (1983)

[14] M. D. Gunzberger, *Perspectives in Flow Control and Optimization*, SIAM, Philadelphia, PA, USA, (2002)

[15] Hoffmann,A., Levchenko,A., Scott, M.L., and Baltimore, D. 'The IκB -NF-κB signaling module:temporal control and selective gene activation', *Science*, **298**, 1241-1245 (2002)

[16] A. Hoffmann, D. Baltimore, Circuitry of nuclear factor kB signaling, *Immunological Reviews*, **210**, 171-186 (2006)

[17] C. Horton, Ph.D Thesis, University of Liverpool (2006).

[18] A.E.C. Ihekwaba, D.S. Broomhead, R.L. Grimley, N. Benson and D.B. Kell 2004 Sensitivity analysis of parameters controlling oscillatory signalling in the NF-κB pathway: the roles of IKK and IκBα *Systems Biology* **1**, pp 93-103.

[19] Karin, M., Yamamoto, Y., and Wang, Q.M.: 'The IKK NF-κB system: a treasure trove for drug development', *Nat. Rev. Drug Discov.,* 2004, **3**, pp 17-26

[20] W. Klonowski, 'Simplifying Principles for Chemical and Enzyme Reaction Kinetics', *Biophysical Chemistry*, **18**, 73–87 (1983)

[21] A. H. Nayfeh, D.T. Mook, *Nonlinear Oscillations*, Wiley, New York, (1979)

[22] D.E. Nelson, A.E.C. Ihekwaba, M. Elliott, J. Johnson, C.A. Gibney, B.E. Foreman, G. Nelson, V. See, C.A. Horton, D.G. Spiller, S.W. Edwards, H.P. McDowell, J.F. Unitt, E. Sullivan, R. Grimley, N. Benson, D. Broomhead, D.B. Kell and M.R.H. White, Oscillations in NF-κB signaling control the dynamics of target gene expression, *Science*, **306**, 704-708 (2004)

[23] G. Nelson et al., *J. Cell Sci.*, **115**, 1137 (2002)

[24] D.A. Rand, B.V. Shulgin, D. Salazar and A.J. Millar 'Design principles underlying circadian clocks', *J.R.Soc. Interface*, **1**, 119–130 (2004)

[25] Sillitoe K, Nelson DE, Horton CA, Ashall L, Johnson JR and White MRH 'Single Cell Timelapse Imaging of the Dynamic Control of NF-κB Signalling', *Biochemical Society Transactions* (2006).

[26] `http://www.math.pitt.edu/ bard/xpp/xpp.html`

[27] E. Zandi, Y. Chen, M. Karin, *Science* **281**, 1360 (1998)